**HORIZON EUROPE PROGRAMME**
HORIZON-CL4-2023-DIGITAL-EMERGING-01-33

GA No. 101135196

# Developing New 2D Materials and Heterostructures for Printed Digital Devices

## 2D-PRINTABLE - Deliverable report

## D1.6 - Other properties of monolayers and multilayers

Funded by
the European Union

| | | |
|---|---|---|
| **Deliverable No.** | D1.6 | |
| **Related WP** | WP 1 | |
| **Deliverable Title** | Other properties of monolayers and multilayers | |
| **Deliverable Date** | 2026-08-21 | |
| **Deliverable Type** | REPORT | |
| **Dissemination level** | Public (PU) | |
| **Author(s)** | Binbin Liu (EPFL)<br>Nicola Marzari (EPFL) | 2026-08-21 |
| **Checked by** | Francesco Bonaccorso (BeD) | 2026-08-23 |
| **Reviewed by** | Ali Shaygan Nia (TUD)<br>Francesco Bonaccorso (BeD) | 2026-08-25 |
| **Approved by** | Jonathan Coleman (TCD) - Project Coordinator | 2026-08-31 |
| **Status** | Final | 2026-08-31 |

**Document History**

| Version | Date | Editing done by | Remarks |
|---|---|---|---|
| V1.0 | 2026-08-21 | Binbin Liu; Nicola Marzari | Initial complete draft |
| V1.1 | 2026-08-25 | Ali Shaygan Nia (TUD)<br>Francesco Bonaccorso (BeD) | revised |
| **FINAL** | 2026-08-31 | Jonathan Coleman (TCD) - Project Coordinator | final |

**Project Scientific Abstract**

The 2D-PRINTABLE project aims to integrate sustainable large-scale liquid exfoliation techniques with theoretical modelling to efficiently produce a wide range of new 2D materials (2DMs), including conducting, semiconducting, and insulating nanosheets. The focus includes developing the printing and liquid phase deposition methods required to fabricate networks and multicomponent heterostructures, featuring layer-by-layer assembly of nanometer-thick 2DMs into ordered multilayers. The goal is to optimize these printed networks and heterostructures for digital systems, unlocking new properties and functionalities. The project also seeks to demonstrate various printed digital devices, including proof-of-principle, first-time demonstration of all-printed, all-nanosheet, heterostack light-emitting diodes (LEDs). In conclusion, 2D-PRINTABLE will prove 2D materials to be an indispensable material class in the field of printed electronics, capable of producing far-beyond-state-of-the-art devices that can act as a platform for the next generation of printed digital applications.

# Public summary

Printable optoelectronic devices require more than a suitable electronic band gap. Candidate nanosheets must also be dynamically stable, retain favourable electronic properties as the layer number changes, and couple efficiently to light. Deliverable D1.6 therefore extends the band-gap screening reported in D1.4 by adding three key descriptors: phonon dispersions, dimensionality-driven indirect-to-direct band-gap crossovers, and polarisation-resolved optical conductivity.

Starting from 2,702 monolayers in the Materials Cloud 2D crystals database (MC2D), the high-throughput workflow applies filters for unit-cell size, magnetism, exfoliability, structural prototype and electronic-gap character. One hundred and forty-two shortlisted monolayers were subjected to protocol-controlled electronic and vibrational calculations, and the final workflow identifies 54 dynamically stable novel direct- or quasi-direct-gap candidates. Density-functional perturbation theory phonon dispersions provide the final stability test by excluding structures with genuine imaginary vibrational modes.

At the PBE level, several stable materials display the sought-after crossover from an indirect bulk parent to a direct or quasi-direct monolayer. Beyond the established MoS2 family, examples include InSiTe3, TeRhCl, YBr3, InBr3, InBrO, Tl2O and Nb(SeCl)2. A detailed layer-resolved Wannier analysis of TeRhCl shows that its bilayer and trilayer remain bulk-like and indirect, whereas the isolated monolayer becomes direct because genuine interlayer hopping channels are suppressed. A subsequent full-zone SOC analysis is used to flag candidates whose directness classification changes when spin-orbit coupling and off-path extrema are included.

Spin-orbit-coupled Wannier calculations were further used to evaluate the optical-conductivity tensor and vacuum-independent two-dimensional response measures. TlPt2Se3, KPt2Se3, PbTe, InSiTe3 and TeRhCl give the largest 1-2 eV conductivity maxima, while HgI2, IrCl3, CuBr, ZrNCl and ZrBrN offer a particularly useful combination of appreciable conductivity and low static in-plane susceptibility. The resulting multi-property shortlist provides concrete priorities for exfoliation, spectroscopy and device prototyping. Absolute gaps and independent-particle optical spectra remain subject to quasiparticle and excitonic corrections, so the highest-priority materials should next be validated with GW/BSE calculations and experiment.

# Contents

# List of Figures



# List of Tables

# Abbreviations & Definitions

| Abbreviation | Explanation |
|---|---|
| **AiiDA** | Automated Interactive Infrastructure and Database for Computational Science |
| **BSE** | Bethe-Salpeter equation |
| **CBM** | Conduction-band minimum |
| **DFT** | Density-functional theory |
| **DFPT** | Density-functional perturbation theory |
| **GW** | Quasiparticle approximation based on the Green function G and screened interaction W |
| **MC2D** | Materials Cloud 2D crystals database |
| **PDOS** | Projected density of states |
| **PL** | Photoluminescence |
| **QE** | Quantum ESPRESSO |
| **SOC** | Spin-orbit coupling |
| **SSSP** | Standard Solid-State Pseudopotentials library |
| **TMD** | Transition-metal dichalcogenide |
| **VBM** | Valence-band maximum |
| **vdW** | van der Waals |

## *Key quantities*

| Quantity | Definition |
|---|---|
| **Eg(fund)** | Fundamental gap between the VBM and CBM, which may occur at different k points. |
| **Eg(dir)** | Minimum vertical (same-k) transition energy over the two-dimensional Brillouin zone. |
| **Delta_dir** | Eg(dir) - Eg(fund); used to distinguish direct, quasi-direct and indirect gaps. |
| **chi_2D** | Vacuum-independent static two-dimensional susceptibility, reported in angstrom. |
| **G_alpha(omega)** | Sheet conductance for polarisation alpha, obtained from the supercell conductivity as L_perp sigma_alphaalpha(omega). |
| **D_Delta** | Integrated in-plane linear dichroism within an optical window Delta. |

# 1 Introduction

Deliverable D1.4 established a broad electronic-structure screening for exfoliable two-dimensional materials and identified monolayers whose gap becomes direct as the number of layers is reduced. D1.6 addresses the next level of validation. A useful photo-active ink must not only have an electronically favourable gap; the isolated layer must be dynamically stable, the desired gap character must survive the relevant thickness range, and the optical matrix elements must generate a sufficiently strong and appropriately polarised response.

Phonon dispersions are the first key validation. A relaxed monolayer can be a stationary point of the total energy while remaining unstable against a collective distortion. Within the harmonic approximation, a genuine imaginary phonon branch signals such instability. Conversely, a spectrum free from imaginary modes, apart from small numerical deviations associated with the long-wavelength flexural acoustic branch, provides reliable first-principles evidence for dynamical stability.

The second extension is a layer-resolved analysis of the indirect-to-direct crossover. In a direct-gap semiconductor, the VBM and CBM occur at the same crystal momentum and radiative recombination does not require phonon assistance. The well-known bulk-to-monolayer crossover in MoS2 enhances photoluminescence by more than an order of magnitude. The present work searches for analogous behaviour beyond the TMD family and, for selected compounds, resolves how interlayer coupling changes the band edges in bilayers, trilayers and the bulk parent.

The third extension is the calculation of the frequency-dependent optical-conductivity tensor. Optical conductivity measures the current induced by an electromagnetic field and therefore retains information that a gap alone cannot provide: oscillator strength, spectral onset, in-plane anisotropy and out-of-plane response. Because a monolayer is represented in a periodic supercell containing vacuum, D1.6 distinguishes the volume-normalised conductivity used to inspect spectra from intrinsic two-dimensional sheet quantities and static susceptibility.

The objectives of D1.6 have been met. The project now has fully traceable and dynamically validated shortlist, a set of physically resolved bulk-to-monolayer crossovers, and an optical-response screen that can guide experimental synthesis and printed-device selection. Remaining uncertainties concern quasiparticle corrections, excitonic effects, finite-temperature stability and environmental compatibility; these are explicitly addressed in Sections 4 and 5.

# 2 Methods and core part of the report

## 2.1 Screening scope and computational provenance

The starting point is the set of 2,702 relaxed monolayers in MC2D, each derived from an experimentally reported layered parent. The screening retains compact unit cells (12 atoms or fewer), non-magnetic or unknown-magnetism entries, and easily exfoliable materials using the binding-energy criteria E_b(DF2) < 30 meV/angstrom^2 or E_b(rVV10) < 35 meV/angstrom^2. A prototype-level filter removes structural families with weak experimental support or prior evidence of monolayer instability. Electronic pre-screening then selects direct- and quasi-direct-gap candidates.

All production calculations are managed through AiiDA workflows interfaced with Quantum ESPRESSO, preserving structures, pseudopotentials, numerical parameters, intermediate calculations and final outputs. Structural relaxations use the protocol-controlled monolayer workflow, followed by PBE electronic-structure calculations with SSSP v1.3 pseudopotentials. The corresponding three-dimensional parent calculations are used for band and orbital comparison; phonon filtering is applied to the monolayers because the parents are experimentally known compounds.

***Table 2.1:*** *Principal screening checkpoints. The intermediate sub-filter counts shown in Figure 2.1 are workflow-version specific; the invariant checkpoints used in D1.6 are 2,702 starting structures, 142 advanced candidates and 54 stable novel candidates.*

| Stage | Retained | Purpose |
|---|---|---|
| **MC2D starting set** | 2,702 | Relaxed monolayers derived from experimentally known parents |
| **Physical and structural pre-screening** | - | Cell size, magnetism, exfoliability and prototype filters |
| **Direct/quasi-direct advanced shortlist** | 142 | Electronic bands, PDOS and phonon calculations |
| **Stable novel candidates** | 54 | Final dynamical-stability and novelty validation |

(a)

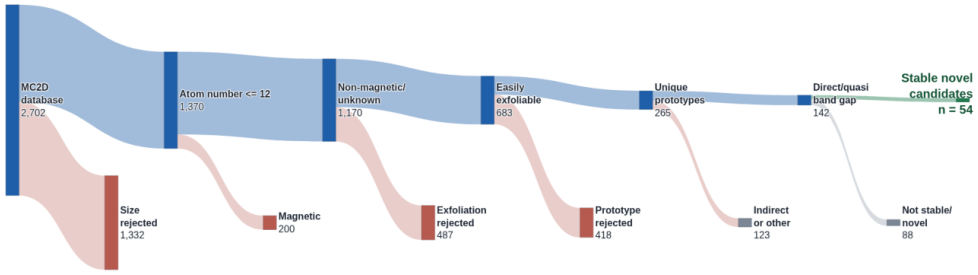


(b)

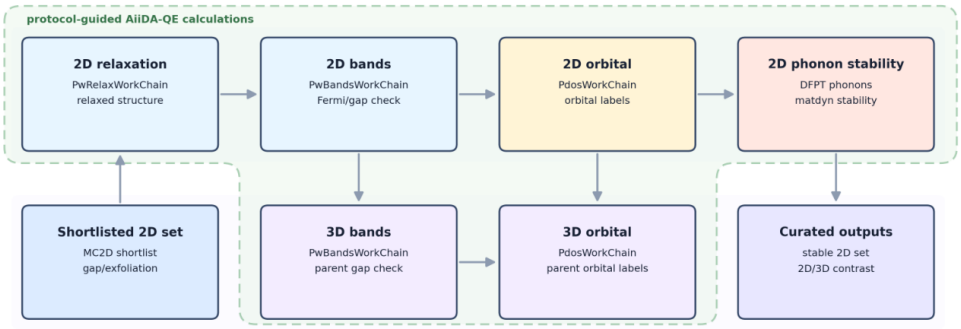


***Figure 2.1:*** *High-throughput screening and calculation workflow. The phonon-dispersion calculation is the final stability filter, while paired 2D/3D electronic and orbital calculations diagnose dimensionality-driven changes.*

## 2.2 Phonon dispersions and dynamical-stability criterion

Phonon dispersions are calculated on top of the fully relaxed monolayer structures using density-functional perturbation theory. A self-consistent ground state is prepared with the same protocol-controlled numerical settings, dynamical matrices are calculated on a reciprocal-space grid, and the real-space force constants are interpolated along the standard two-dimensional high-symmetry path. The calculation retains the three acoustic branches required by translational invariance, including the quadratic flexural ZA branch near Gamma.

A material is classified as dynamically stable when no physically significant imaginary branch is present. The automated screen applies a tolerance of -0.05 THz to avoid rejecting structures because of minute interpolation or acoustic-sum-rule noise at Gamma. Candidates with larger or extended negative-frequency branches are excluded. Borderline cases are reserved for stricter q-mesh, supercell or finite-temperature checks rather than promoted to the final list.

## 2.3 Direct, quasi-direct and indirect-gap classification

The initial scalar-relativistic classification is obtained from band structures along symmetry-aware high-symmetry paths. The fundamental gap and minimum direct transition are defined as

$$E_g(\mathrm{fund}) = E_c(k_c) - E_v(k_v), \qquad E_g(\mathrm{dir}) = \min_k [E_c(k) - E_v(k)], \qquad \Delta_{\mathrm{dir}} = E_g(\mathrm{dir}) - E_g(\mathrm{fund}).$$

On a finite path, a gap is treated as direct when the sampled VBM and CBM are separated by less than 0.08 angstrom^-1. If the minimum direct transition is within 60 meV of the fundamental gap, the system is labelled quasi-direct; all remaining semiconductors are indirect. Quasi-direct materials are retained because thermal broadening and excitonic effects can make their optical behaviour similar to that of a strictly direct semiconductor.

For the optical-production subset, fully relativistic SOC Wannier Hamiltonians are searched over the complete two-dimensional Brillouin zone. In this stricter full-zone classification, Delta_dir <= 1 meV denotes a direct gap, 1 meV < Delta_dir <= 60 meV a quasi-direct gap, and larger values an indirect gap. This step removes the risk that an off-path extremum changes the assignment and also captures SOC-induced changes in heavy-element compounds.

## 2.4 SOC-Wannier optical-conductivity workflow

Fully relativistic non-collinear PBE calculations are Wannierised with projectability-based disentanglement and external projectors where needed. The spinor Wannier Hamiltonians are validated against the corresponding Quantum ESPRESSO bands and then used both for the full-zone gap search and for independent-particle optical calculations with the postw90 Kubo module.

The in-plane reciprocal-space mesh targets a spacing of approximately 0.01 angstrom^-1. The optical spectra use a fixed Gaussian broadening of 0.02 eV and an energy step of 0.0025 eV. The calculated diagonal tensor components are Re sigma_xx(hbar omega), Re sigma_yy(hbar omega) and Re sigma_zz(hbar omega). Near-edge spectral weights are integrated in windows of 0.10, 0.25 and 0.50 eV above Eg(dir), and the in-plane linear dichroism D_Delta = (W_x - W_y)/(W_x + W_y) quantifies polarisation anisotropy. Static chi_2D is used as a vacuum-independent indicator of polarisation and refractive response. The S/cm values plotted in this report remain useful for comparing spectra calculated with the same supercell convention, but sheet conductance and chi_2D are the transferable two-dimensional quantities. The present spectra do not include electron-hole interactions.

# 3 Results & Discussion

## 3.1 Phonon-stable monolayers

The DFPT calculation is a key selection criterion. Electronic structure and phonon spectra were calculated for the advanced shortlist of 142 monolayers, and the combined stability and novelty validation leaves 54 novel direct- or quasi-direct-gap candidates. The supporting catalogue retains additional reference and comparison systems so that the full screening path remains auditable.

The stable set spans chemically and mechanically distinct families. Figure 3.1 illustrates four representative vibrational spectra. MoS2 provides the established TMD reference and reaches optical branches near 14 THz. Heavy-element HgI2 has a much softer spectrum below roughly 4 THz. TeRhCl combines several low-frequency branches with an upper manifold near 8 THz, whereas ZrNCl extends above 20 THz. In each example the acoustic branches approach zero at Gamma without an extended imaginary branch.

This diversity matters for printed devices. Softer lattices can enhance electron-phonon scattering and temperature sensitivity, while high-frequency optical modes can influence non-radiative relaxation and Raman fingerprints. D1.6 does not yet rank carrier mobility or non-radiative rates, but the dispersions provide the necessary starting point for those calculations and for experimental Raman/infrared identification.

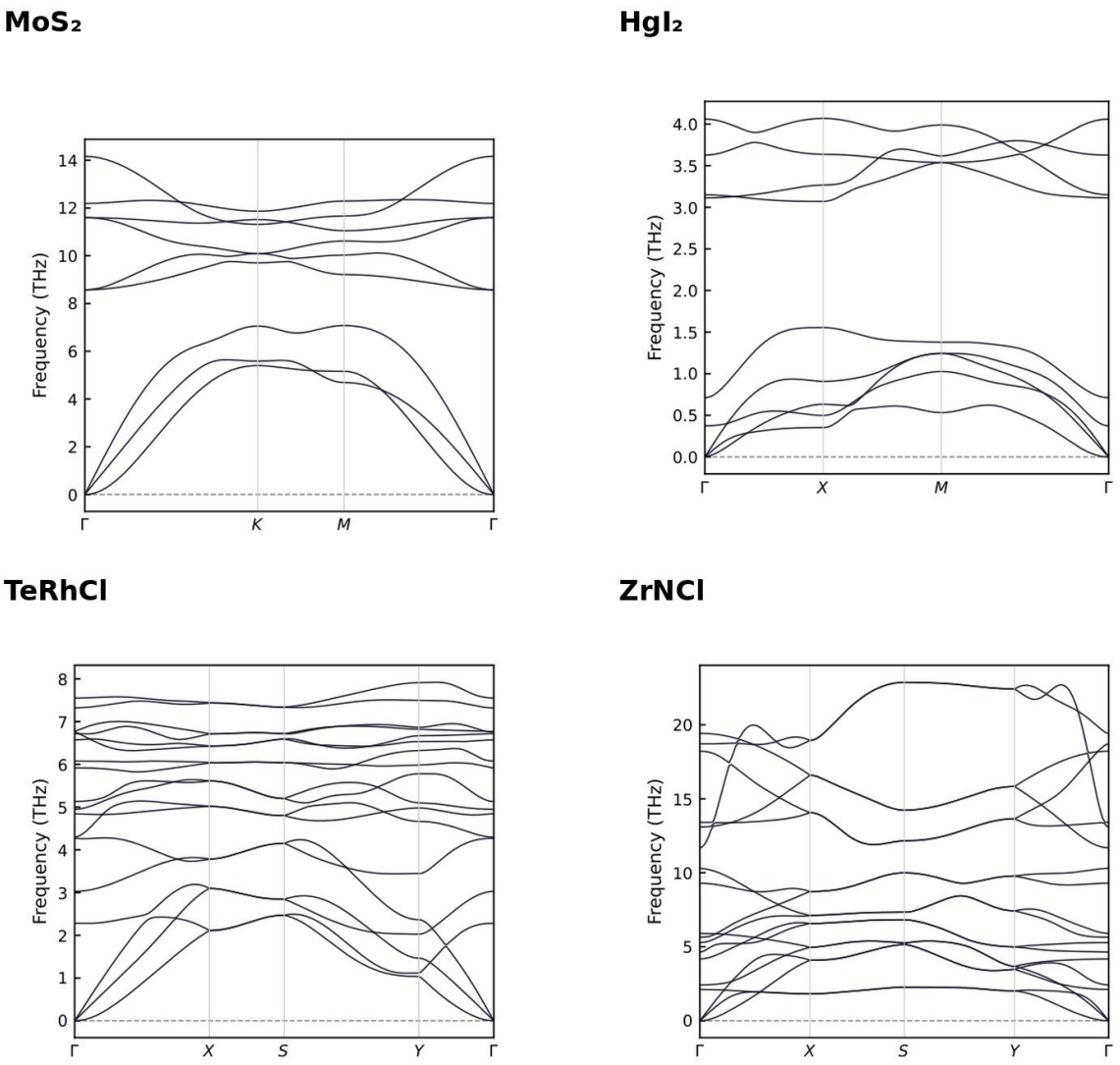


***Figure 3.1:*** *Representative phonon dispersions of dynamically stable monolayers. The panels demonstrate the broad vibrational-frequency range covered by the shortlist, from soft heavy-element systems to stiff nitride-halides.*

## 3.2 Indirect-to-direct band-gap crossovers

The most relevant PBE-level crossovers are those in which an experimentally known indirect-gap bulk parent produces a stable direct or quasi-direct monolayer. Table 3.1 lists representative results. InSiTe3, TeRhCl and YBr3 are novel non-TMD examples with direct monolayer gaps in the scalar-relativistic workflow. InBr3, InBrO, Tl2O, Nb(SeCl)2 and HfS3 become quasi-direct. The established WS2, MoS2 and MoSe2 cases are included as internal references.

Most crossovers are accompanied by a larger monolayer gap, as expected from reduced screening and quantum confinement. The magnitude of the change is nevertheless material-specific, and a directness crossover should not be inferred from the gap increase alone. Orbital-resolved bands and PDOS show that many candidates redistribute transition-metal d and ligand p character at the band edges as the out-of-plane coupling is removed.

***Table 3.1:*** *Selected phonon-stable bulk-to-monolayer crossovers. Classifications and gaps are PBE-level workflow values; BE is the DF2-C09 binding energy. The SOC full-zone classification used for optical screening can differ for borderline and heavy-element materials.*

| 2D material | 2D class | Eg 2D (eV) | 3D class | Eg 3D (eV) | Delta Eg (eV) | BE (meV/A2) |
|---|---|---|---|---|---|---|
| **InSiTe3** | direct | 0.85 | indirect | 0.10 | +0.75 | 18.5 |
| **TeRhCl** | direct | 1.07 | indirect | 0.45 | +0.62 | 19.2 |
| **YBr3** | direct | 4.13 | indirect | 3.68 | +0.45 | 5.5 |
| **InBr3** | quasi-direct | 3.04 | indirect | 2.19 | +0.85 | 9.8 |
| **InBrO** | quasi-direct | 2.45 | indirect | 1.87 | +0.57 | 9.6 |
| **Tl2O** | quasi-direct | 0.74 | indirect | 0.37 | +0.37 | 19.4 |
| **Nb(SeCl)2** | quasi-direct | 1.04 | indirect | 0.83 | +0.21 | 13.6 |
| **HfS3** | quasi-direct | 1.03 | indirect | 0.93 | +0.10 | 19.5 |
| **WS2** | direct | 1.99 | indirect | 0.91 | +1.08 | 22.7 |
| **MoS2** | direct | 1.82 | indirect | 0.84 | +0.98 | 21.6 |
| **MoSe2** | direct | 1.59 | indirect | 0.81 | +0.78 | 20.4 |

TeRhCl is the clearest non-TMD microscopic case study. The bulk parent has an indirect PBE gap of 0.45 eV, whereas the isolated monolayer has a direct gap of 1.07 eV. Layer-resolved Wannier slabs retain an indirect gap for three layers (about 0.70 eV) and two layers (about 0.88 eV), so the crossover occurs only at the monolayer limit. The specific conventional-cell/Wannier panel annotations in Figure 3.2 report 0.41 and 1.18 eV; the small difference from the workflow table reflects the distinct representation and post-processing used for the layer-resolved analysis.

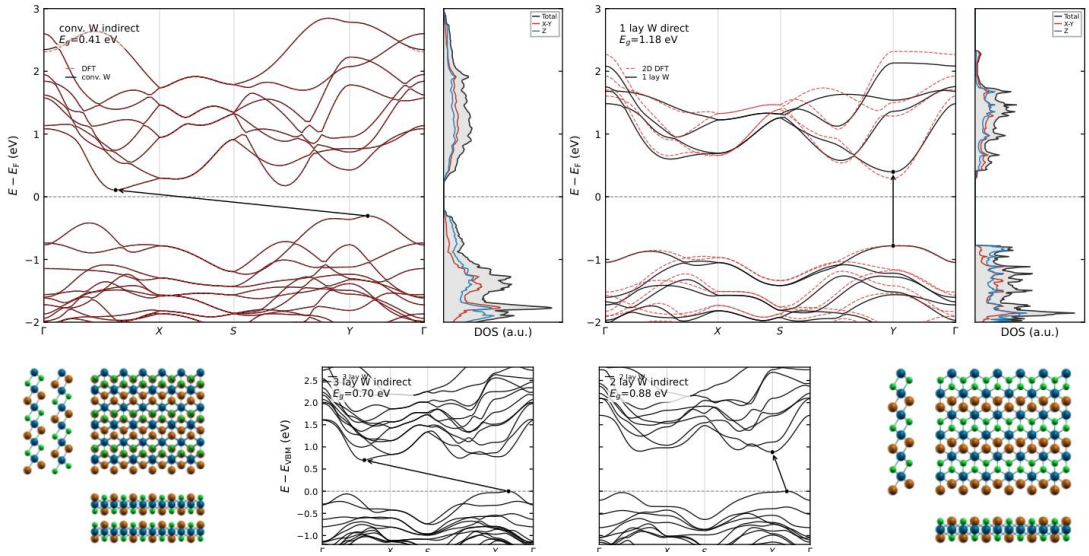


***Figure 3.2:*** *TeRhCl layer-dependent crossover. Bulk, trilayer and bilayer retain an indirect gap, while the monolayer becomes direct. Wannier-interpolated bands reproduce the DFT bands and permit a controlled removal of interlayer hopping channels.*

The Hamiltonian analysis identifies the loss of genuine interlayer hopping as the origin of the crossover. In the conventional bulk Hamiltonian, the nearest c-axis hopping sector has a Frobenius norm of 2.14 eV and a largest element of 0.588 eV, dominated by Te/Cl p-derived states hybridised with Rh d states. In the one-layer cut, the corresponding out-of-plane sector is reduced to a norm of 0.742 eV and a

maximum element of 0.186 eV. Subtracting the two-layer slab Hamiltonian from the bulk further isolates the genuine out-of-plane contribution, confirming that the in-plane network is largely preserved.

A complementary group of compounds is dimensionally robust rather than crossover-driven. ZrBrN, ZrNCl, HfBrN and TiNCl remain direct in both bulk and monolayer, with changes of only a few hundredths of an electronvolt. These FeOCl-prototype nitride-halides are attractive when device reproducibility across a distribution of nanosheet thicknesses is more important than an abrupt monolayer-only enhancement.

The SOC full-zone analysis is kept separate from the PBE crossover table. In the current optical batch, InBr3 and InBrO become direct, YBr3 and Tl2O remain quasi-direct, while InSiTe3 and TlPt2Se3 are classified as indirect once SOC and off-path extrema are included. TeRhCl remains direct. This distinction prevents a high optical-conductivity value from being interpreted automatically as evidence of a strictly direct SOC gap.

## 3.3 Optical conductivity and static 2D susceptibility

The SOC-Wannier optical calculations add oscillator strength and polarisation selection rules to the gap-based shortlist. The MoS2 benchmark gives a full-zone minimum direct gap of 1.582 eV, an in-plane static chi_2D of approximately 6.51 angstrom, a 1-2 eV in-plane conductivity maximum of about 538 S/cm at 1.906 eV, and a larger independent-particle peak near 2.866 eV. Agreement of the calculated spectral structure with the reference benchmark supports the use of the same workflow for the less explored candidates.

Two complementary rankings are useful. The first identifies the largest 1-2 eV conductivity maxima, irrespective of static screening. TlPt2Se3 is the strongest, followed by KPt2Se3, PbTe, InSiTe3 and TeRhCl. The second restricts attention to chi_2D at or below the median of the completed optical set, 2.82 angstrom. Within this low-susceptibility subset, HgI2 and IrCl3 provide the strongest response; CuBr has the smallest chi_2D and a well-resolved internal maximum at 1.68 eV; ZrNCl and ZrBrN retain appreciable conductivity with moderate static screening.

Maxima reported at exactly 2.00 eV should be interpreted as the largest value within the selected 1-2 eV interval, because the spectrum can still be rising at the upper boundary. The table therefore records both the amplitude and the peak energy. It also separates the high-response and low-susceptibility objectives rather than collapsing them into a single arbitrary score.

***Table 3.2:*** *Optical-response screening in the 1-2 eV range. Conductivity is the in-plane mean of the supercell-normalised postw90 spectra; chi_2D is the vacuum-independent static in-plane susceptibility. SOC class is obtained from the full-zone Wannier search.*

| Screen | Material | SOC class | Eg(dir), SOC | max sigma 1-2 | Epeak | chi_2D |
|---|---|---|---|---|---|---|
| **High response** | TlPt2Se3 | indirect | 1.25 | 1826.1 | 1.959 | 6.73 |
| **High response** | KPt2Se3 | direct | 1.13 | 1099.2 | 1.999 | 5.56 |
| **High response** | PbTe | direct | 1.08 | 1084.5 | 1.815 | 4.82 |
| **High response** | InSiTe3 | indirect | 0.87 | 1080.9 | 1.965 | 6.74 |
| **High response** | TeRhCl | direct | 1.09 | 973.8 | 1.996 | 4.74 |

| Screen | Material | SOC class | Eg(dir), SOC | max sigma 1-2 | Epeak | chi_2D |
|---|---|---|---|---|---|---|
| Low chi_2D | HgI2 | direct | 1.54 | 257.7 | 1.996 | 1.67 |
| Low chi_2D | IrCl3 | quasi-direct | 1.83 | 232.9 | 2.000 | 1.40 |
| Low chi_2D | ZrNCl | direct | 1.85 | 124.2 | 1.996 | 2.48 |
| Low chi_2D | ZrBrN | direct | 1.81 | 107.2 | 1.996 | 2.77 |
| Low chi_2D | CuBr | direct | 1.50 | 88.0 | 1.680 | 1.10 |

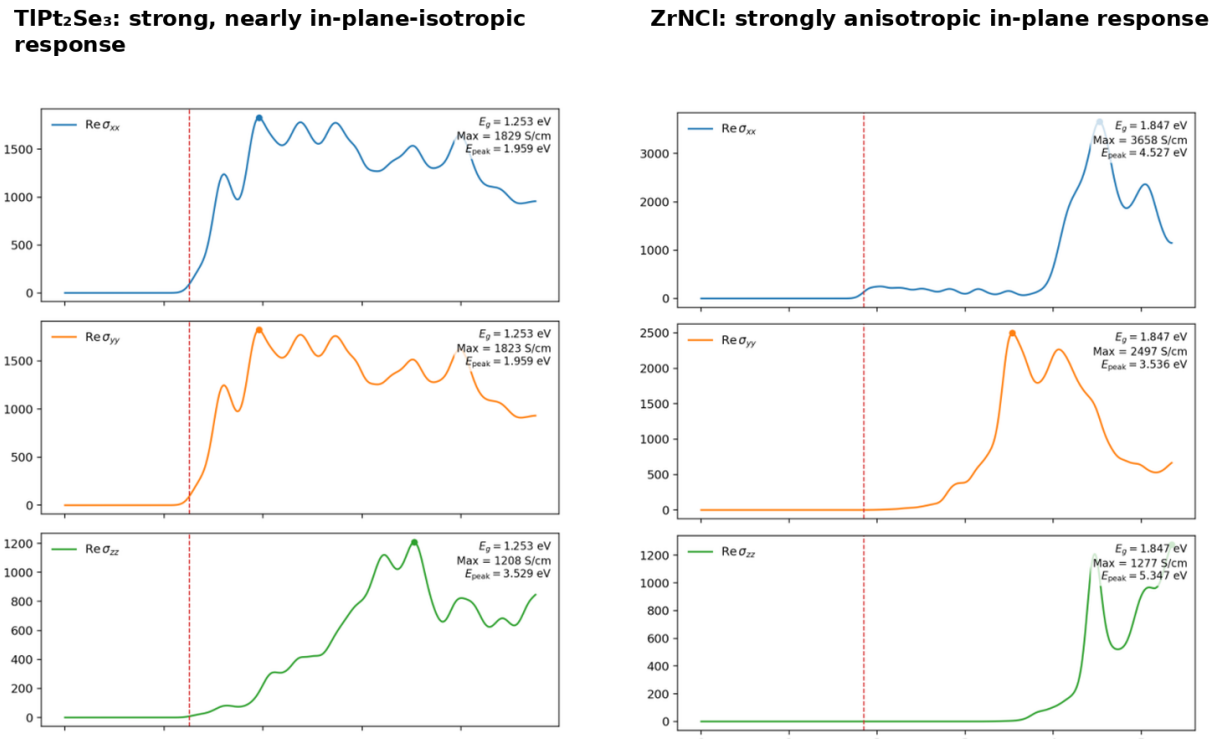


***Figure 3.3:*** *Representative SOC-Wannier optical-conductivity tensors. TlPt2Se3 combines a strong and nearly isotropic in-plane response near 2 eV, whereas ZrNCl displays pronounced x/y anisotropy. The dashed line marks the minimum direct gap; the spectra are independent-particle results.*

The contrast between these materials illustrates why tensor information is essential. TlPt2Se3 has a 1-2 eV maximum of 1826 S/cm and negligible integrated in-plane dichroism in the 0.50 eV near-edge window. ZrNCl has a lower 1-2 eV maximum of 124 S/cm but a dichroism of approximately 0.92, making it a candidate for polarisation-sensitive detection. Out-of-plane spectral weight is small near the gap for most candidates, as expected for an atomically thin layer, but becomes appreciable at higher photon energies in some heavy-element systems.

## 3.4 Cross-property prioritisation

No single descriptor can define the best printable semiconductor. Table 3.3 combines the three themes of D1.6 with exfoliability and application context. The recommendations are priorities for follow-up, not final device rankings: ink formulation, defect tolerance, environmental stability, band alignment and processing compatibility remain to be tested.

***Table 3.3:*** *Cross-property priorities for experimental and higher-level theoretical follow-up.*

| Material | Electronic/phonon result | Optical discriminator | Recommended next step |
|---|---|---|---|
| TeRhCl | Stable; monolayer-only direct crossover; SOC direct | 973.8 S/cm; chi_2D 4.74 A | GW/BSE, layer-resolved PL and thickness control |

| Material | Electronic/phonon result | Optical discriminator | Recommended next step |
|---|---|---|---|
| **InSiTe3** | PBE direct crossover; SOC full-zone indirect | 1080.9 S/cm; chi_2D 6.74 A | Resolve SOC extrema; near-IR/visible absorption and stability |
| **TlPt2Se3** | Metal parent to PBE quasi-direct; SOC indirect | Strongest 1-2 eV response; high screening | Exfoliation, transport and contact engineering |
| **HgI2** | Stable direct gap; soft lattice | 257.7 S/cm; low chi_2D 1.67 A | Flexible photodetection and excitonic spectrum |
| **IrCl3** | Stable SOC quasi-direct optical candidate | 232.9 S/cm; low chi_2D 1.40 A | SOC/excitonic validation and magnetic checks |
| **ZrNCl** | Dimensionally robust direct gap; stiff lattice | 124.2 S/cm; dichroism about 0.92 | Polarisation-resolved optics and thickness-tolerant devices |
| **InBr3** | PBE quasi-direct crossover; SOC direct | Low chi_2D about 1.2 A; UV response | UV emitter/detector and halide stability |

## 3.5 Contribution to project objectives and exploitable results

D1.6 contributes directly to the WP1 materials objective of combining theoretical modelling with growth and large-scale liquid exfoliation to produce new conducting, semiconducting and insulating nanosheets with targeted electronic and optical properties. Relative to D1.4, the present deliverable reduces the risk of forwarding electronically attractive but dynamically unstable compounds and adds optical metrics that are directly relevant to photoluminescence, LEDs, photodetectors and photovoltaic absorbers.

The major exploitable result is a reproducible multi-property discovery workflow and its curated candidate set. The AiiDA provenance, per-material phonon and PDOS catalogue, layer-resolved Wannier models and SOC optical-response outputs are scientific data assets that can be used by the experimental partners to select targets and by the device work packages to identify suitable active, transparent or anisotropic layers.

No potentially patentable foreground IP has been identified by the authors at this screening stage. The principal outputs are workflows, datasets and scientific discoveries; ownership, release and publication will follow the Consortium Agreement and the project data-management plan. The TeRhCl mechanism and the broader stable direct-gap landscape are being prepared for scientific publication.

# 4 Conclusion and Recommendation

D1.6 completes the requested extension from band-gap screening to other properties of monolayers and multilayers. The high-throughput workflow subjects 142 advanced candidates to electronic, orbital and vibrational characterisation and yields 54 dynamically stable novel direct- or quasi-direct-gap monolayers. The phonon catalogue demonstrates that the resulting set covers a broad range of lattice stiffness and chemical families while passing the harmonic stability criterion.

The dimensionality analysis identifies both monolayer-only crossovers and thickness-robust semiconductors. TeRhCl provides a microscopic non-TMD example: bulk, trilayer and bilayer remain indirect, while removing the final interlayer hopping channels produces a direct monolayer gap. Conversely, ZrNCl and related nitride-halides retain their direct character across thickness, which may be advantageous for liquid-exfoliated inks containing a distribution of layer numbers.

The optical-conductivity screen separates strong absorption from low static response and from anisotropy. TlPt2Se3 and TeRhCl are high-response priorities, with the caveat that TlPt2Se3 is indirect in the current SOC full-zone classification; HgI2 and IrCl3 offer a favourable low-susceptibility balance; ZrNCl is especially interesting for polarisation-selective devices. These results provide an actionable short list rather than a gap-only ranking.

### *Recommended next actions*

- Prioritise TeRhCl, HgI2, IrCl3, ZrNCl and TlPt2Se3 for experimental exfoliation and spectroscopy, while using InSiTe3 as a high-response candidate whose SOC directness requires further resolution and InBr3 as a wide-gap/UV target.
- Perform converged GW and SOC-BSE calculations for the leading visible-range and heavy-element candidates; the existing GW results for TeRhCl and HfBrN provide the first validation points.
- Use Raman and infrared measurements to confirm the calculated phonon fingerprints and to detect possible substrate- or temperature-induced instabilities.
- Measure thickness-dependent photoluminescence/absorption for crossover candidates and polarisation-resolved response for anisotropic materials such as ZrNCl.
- Retain sheet conductance and chi_2D, rather than an arbitrary effective bulk refractive index, when comparing isolated monolayers and printed nanosheet networks.

# 5 Risks and interconnections

## 5.1 Risks/problems encountered

The principal technical risks and their mitigation are summarised below. Probability and effect use the project scale 1 = high, 2 = medium and 3 = low.

***Table 5.1:*** *Technical risks and mitigation measures for the calculations and interpretation reported in D1.6.*

| Risk No. | What is the risk | Probability | Effect | Solutions to overcome the risk |
|---|---|---|---|---|
| **WP1.6-R1** | Small imaginary acoustic frequencies can arise from interpolation, finite q meshes or incomplete acoustic-sum-rule enforcement. | 2 | 2 | Use the -0.05 THz numerical tolerance; repeat borderline cases with denser q meshes, stricter convergence, larger cells and finite-temperature checks. |
| **WP1.6-R2** | High-symmetry paths can miss off-path band extrema and change direct/quasi-direct assignments. | 2 | 2 | Validate priority candidates with full-Brillouin-zone SOC Wannier searches and continuous extremum refinement. |
| **WP1.6-R3** | PBE gaps are lower bounds and independent-particle spectra omit excitonic effects. | 1 | 2 | Apply GW and SOC-BSE to the leading candidates; benchmark against MoS2 and experimental PL/reflectivity. TeRhCl and HfBrN already have GW checks. |
| **WP1.6-R4** | Supercell-normalised S/cm conductivity and an assumed monolayer thickness can lead to misleading cross-study comparisons. | 2 | 2 | Report vacuum-independent sheet conductance and chi_2D; record L_perp and the vacuum gap; avoid assigning a bulk refractive index unless a thickness convention is explicit. |
| **WP1.6-R5** | Dynamic stability at 0 K does not guarantee chemical, substrate or processing stability in liquid-exfoliated inks. | 2 | 1 | Combine the calculated shortlist with experimental ageing, solvent, oxidation and substrate tests; use encapsulation or chemical substitution where necessary. |

## 5.2 Interconnections with other deliverables

D1.6 is a direct continuation of D1.4, which established the monolayer/multilayer band-gap landscape and the initial indirect-to-direct screen. The present phonon filter, SOC reclassification and optical-response analysis refine that list and supply the physical evidence required to prioritise stable optoelectronic candidates.

The results provide direct input to D1.5, Production of novel 2D nanosheets, by identifying experimentally known parents with favourable binding energies and stable monolayer dispersions. They also inform downstream printed-device activities by distinguishing high-absorption materials, low-screening layers, polarisation-sensitive candidates and thickness-robust systems.

The machine-readable outputs and supporting catalogue are designed to be reused in later calculations of excitons, mobility, electron-phonon coupling, heterostructure band alignment and network-level optical response.

# 6 Deviations from Annex 1

No deviations from Annex 1 are reported. The work extends the planned electronic-property screening with the phonon-stability and optical-response validation required by the deliverable title.

# 7 References


**1.** Mounet, N.; et al. Two-dimensional materials from high-throughput computational exfoliation of experimentally known compounds. Nature Nanotechnology 2018, 13, 246-252.

**2.** Campi, D.; Mounet, N.; Gibertini, M.; Pizzi, G.; Marzari, N. The Materials Cloud 2D database (MC2D). Materials Cloud Archive 2022.

**3.** Giannozzi, P.; et al. QUANTUM ESPRESSO: a modular and open-source software project for quantum simulations of materials. Journal of Physics: Condensed Matter 2009, 21, 395502.

**4.** Giannozzi, P.; et al. Advanced capabilities for materials modelling with Quantum ESPRESSO. Journal of Physics: Condensed Matter 2017, 29, 465901.

**5.** Pizzi, G.; Cepellotti, A.; Sabatini, R.; Marzari, N.; Kozinsky, B. AiiDA: automated interactive infrastructure and database for computational science. Computational Materials Science 2016, 111, 218-230.

**6.** Huber, S. P.; et al. AiiDA 1.0, a scalable computational infrastructure for automated reproducible workflows and data provenance. Scientific Data 2020, 7, 300.

**7.** Perdew, J. P.; Burke, K.; Ernzerhof, M. Generalized Gradient Approximation Made Simple. Physical Review Letters 1996, 77, 3865-3868.

**8.** Prandini, G.; Marrazzo, A.; Castelli, I. E.; Mounet, N.; Marzari, N. Precision and efficiency in solid-state pseudopotential calculations. npj Computational Materials 2018, 4, 72.

**9.** Monkhorst, H. J.; Pack, J. D. Special points for Brillouin-zone integrations. Physical Review B 1976, 13, 5188-5192.

**10.** Mostofi, A. A.; et al. wannier90: A tool for obtaining maximally-localised Wannier functions. Computer Physics Communications 2008, 178, 685-699.

**11.** Pizzi, G.; et al. Wannier90 as a community code: new features and applications. Journal of Physics: Condensed Matter 2020, 32, 165902.

**12.** Mak, K. F.; Lee, C.; Hone, J.; Shan, J.; Heinz, T. F. Atomically Thin MoS2: A New Direct-Gap Semiconductor. Physical Review Letters 2010, 105, 136805.

**13.** Splendiani, A.; et al. Emerging Photoluminescence in Monolayer MoS2. Nano Letters 2010, 10, 1271-1275.

**14.** Li, Y.; et al. Measurement of the optical dielectric function of monolayer transition-metal dichalcogenides: MoS2, MoSe2, WS2, and WSe2. Physical Review B 2014, 90, 205422.

**15.** Wang, G.; et al. Colloquium: Excitons in atomically thin transition metal dichalcogenides. Reviews of Modern Physics 2018, 90, 021001.

**16.** Hybertsen, M. S.; Louie, S. G. Electron correlation in semiconductors and insulators: Band gaps and quasiparticle energies. Physical Review B 1986, 34, 5390-5413.

**17.** Golze, D.; Dvorak, M.; Rinke, P. The GW Compendium: A Practical Guide to Theoretical Photoemission Spectroscopy. Frontiers in Chemistry 2019, 7, 377.

**18.** Liu, B.; Marzari, N. High-throughput identification of novel direct-gap 2D semiconductors and the indirect-to-direct crossover. Manuscript in preparation, 2026.

**19.** Liu, B.; Marzari, N. Electronic and Phonon Band Structures for Short-Listed 2D Materials. Supporting technical catalogue, 19 August 2026.

**20.** 2D-PRINTABLE Deliverable D1.4. Band gaps of monolayers and multilayers. EPFL, 2025.

# 8 Acknowledgement

The author(s) would like to thank the partners in the project for their valuable comments on previous drafts and for performing the review.

**Project partners:**

| # | Partner short name | Partner Full Name |
|---|---|---|
| **1** | TCD | TCD THE PROVOST, FELLOWS, FOUNDATION SCHOLARS & THE OTHER MEMBERS OF BOARD, OF THE COLLEGE OF THE HOLY & UNDIVIDED TRINITY OF QUEEN ELIZABETH NEAR DUBLIN |
| **2** | UNISTRA | UNIVERSITE DE STRASBOURG |
| **3** | UKa | UNIVERSITAET KASSEL |
| **4** | BED | BEDIMENSIONAL SPA |
| **5** | TUD | TECHNISCHE UNIVERSITAET DRESDEN |
| **6** | VSCHT | VYSOKA SKOLA CHEMICKO-TECHNOLOGICKA V PRAZE |
| **7** | UNR | UNIRESEARCH BV |
| **8** | UniBw M | UNIVERSITAET DER BUNDESWEHR MUENCHEN |
| **9** | EPFL | ECOLE POLYTECHNIQUE FEDERALE DE LAUSANNE |

## *Disclaimer/ Acknowledgment*



This project has received funding from the European Union's Horizon Europe research and innovation programme under grant agreement No 101135196. Views and opinions expressed are however those of the author(s) only and do not necessarily reflect those of the European Union. Neither the European Union nor the granting authority can be held responsible for them.

# 9 Appendix B - Supporting catalogue and data provenance

The supporting technical catalogue contains per-material electronic bands, projected densities of states, crystal structures, phonon dispersions and, where completed, SOC-Wannier optical-response diagnostics. The catalogue is sorted by the monolayer-to-parent gap change and retains MC2D identifiers and AiiDA provenance, allowing every result summarised in this deliverable to be traced to the corresponding calculation. The full catalogue and machine-readable workflow outputs are maintained by EPFL and will be disseminated according to the project publication and data-management plan.